Fin Induced Laminar Interactions on Sharp and Spherically Blunted Cones

T. TAZ BRAMLETTE*
Sandia Laboratories, Livermore, Calif.

AND

RICHARD R. SMITH† AND NEIL J. SLISKI†
Air Force Flight Dynamics Laboratory, Wright Patterson Air Force Base, Ohio

The flowfield structure (surface streamlines and shock patterns), and pressure and heat-transfer distributions associated with small fins mounted near the base of a 7° half-angle cone are measured. The tests are conducted in a hypersonic freestream at a Mach number of 10, freestream unit Reynolds numbers of 0.12 and 0.6 × 10^6/foot, and wall to total temperature ratio of 0.27. Vehicle geometry (nose bluntness, and fin sweep, shape, thickness, and cant) and orientation (angles of attack and roll) are systematically varied. Fin leading-edge pressure and heat transfer agree with swept infinite cylinder predictions; fin side heating agrees with blunt swept slab theory. Flow patterns, heating and pressure in the fin-cone region are characteristic of corner flow geometries.

Nomenclature

b = skin thickness
c = heat capacity; constant
d = fin thickness
F = empirically determined function of $\bar{\chi}$, M, δ
G = empirically determined function of $\bar{\chi}$, M, Λ
h = heat-transfer coefficient, Btu/ft²-sec-°F
L = model length, in.
M = Mach number
P = pressure
$\dot{q}$ = heat-transfer rate, Btu/ft²-sec
r, R = radius, in.
Rey_∞ = freestream unit Reynolds number, per ft
$Rey_{\infty,x}$ = freestream Reynolds number based on x
$Rey_{c,x}$ = cone shock layer Reynolds number based on x
s = surface distance measured from fin stagnation line parallel to cone surface
t = time
x = surface distance measured from cone stagnation point
x', y' = local coordinate system with origin at forward location of fin induced separation
z = surface distance measured from fin leading edge/cone surface intersection parallel to fin leading edge
α = angle of attack, deg
Δ = separation distance
δ = fin cant, deg; flap deflection, deg
θ_c = cone half-angle, deg
Λ = fin leading edge sweep, deg
ρ = thin-skin density
ϕ = roll angle, deg
$\bar{\chi}$ = viscous interaction parameter

Subscripts

b = base
c = cone
f = fin side
n, N = nose
o = stagnation
s = stagnation line
w = wall; windward meridian
∞ = freestream

Presented as Paper 73-235 at the AIAA 11th Aerospace Sciences Meeting, Washington, D.C., January 10–12, 1973; submitted February 20, 1973; revision received June 25, 1973. This work was supported by the U.S. Atomic Energy Commission and U. S. Air Force.

Index categories: Boundary Layers and Convective Heat Transfer—Laminar; Jets, Wakes, and Viscid-Inviscid Flow Interactions; Supersonic and Hypersonic Flow.

* Member of Technical Staff, Aerothermodynamics Division. Member AIAA.

† Members of Technical Staff, High Speed Aero Performance Branch.

I. Introduction

FOR certain classes of reentry vehicles (RV), anomalous roll-rates can be experienced which may result in structural damage to and/or performance degradation of the *RV* (this phenomenon is termed roll-resonance). One concept being considered to eliminate this problem consists of using small fins located on the aft portion of the vehicle to control the roll-rate (characteristic heights and widths are about three to four times the local boundary-layer thickness). Since roll-rate excursions are often experienced at altitudes of about 100,000 ft, the first roll resonance condition may occur in the laminar flow regime.

Because of its practical significance, the laminar flow regime has been the subject of numerous studies. The configurations which have been studied that are relevant to the present investigation have included sharp and spherically blunted cones[1–7], sharp and blunt fins of varying sweep,[8–11] and various corner flow geometries[12–17]. A fairly complete understanding of hypersonic, laminar interactions has emerged from these studies, although in many cases theoretical prediction techniques are lacking. An excellent review of viscous interactions associated with flight at high Mach numbers is given in Ref. 18.

For the present configuration, which is a sphere-cone, two mechanisms may lead to viscous interaction: 1) fin induced interaction with the vehicle boundary layer, and 2) angle of attack induced boundary-layer separation from the leeward side of the cone. Both types of interaction modify local vehicle surface pressures, and may be accompanied by significant increases in local heat-transfer rates. The present study was undertaken to characterize the flowfield, pressure.

and heat transfer associated with these interactions on a finned reentry vehicle in laminar, hypersonic flow.

The experimental program was divided into three phases: flowfield visualization, pressure measurement, and heat-transfer measurement. The flowfield visualization portion of the study consisted of oil tests to establish surface streamline patterns and delineate regions of separated flow, and schlieren observations to establish the nature of the shock wave patterns. The pressure phase consisted of measurements of pressures on the fin leading edge and side and on the cone surface in the vicinity of the fin. Two types of measurements were taken during the heat-transfer phase. Leading-edge heat-transfer rates were obtained with the transient thin-skin technique; heat-transfer rates in the vicinity of the fin were obtained with the phase change paint technique. During each phase of the study, freestream conditions, vehicle orientation (angles of attack and roll), and vehicle geometry (nose bluntness, fin sweep, shape, thickness, and cant) were systematically varied.

II. Facility, Models, and Experimental Techniques

Facility

The tests were conducted in the Air Force Flight Dynamics Lab. (AFFDL) High Temperature Facility. This facility is a hypersonic blowdown wind tunnel which uses an alumina pebble bed heater as its high temperature source. For the present tests, the contoured axisymmetric Mach 10 nozzle was utilized. Nominal stagnation conditions were $T_0 = 2100°R(T_w/T_0 \approx 0.27)$, and $P_0 = 100$ and 600 psia. These conditions provided freestream Reynolds numbers based on the sharp cone length of 0.2 and 1×10^6, respectively. Additional facility information is contained in Refs. 19 and 20.

Model

Sketches of the wind-tunnel model and the coordinate system adopted in the present study are presented in Fig. 1. The model was a 7° half-angle cone with interchangeable sharp and blunt nose tips ($r_n/r_b = 0$ and 0.104). Two models were constructed: 1) a Teflon model for the heat-transfer tests, and 2) a stainless steel model for the pressure and oil flow tests. Each of these cones was fitted with interchangeable fins. The basic fin was swept 60° from the normal, had a cylindrical leading edge, and a length, height and width of 1.83, 0.5, and 0.3 in., respectively. Additional fins were utilized to investigate the effects of thickness ($d = 0.5$ in.), sweep ($\Lambda = 45°$) and leading edge shape (flat). In addition to the Teflon fins, two instrumented fins for pressure and heat transfer were constructed.

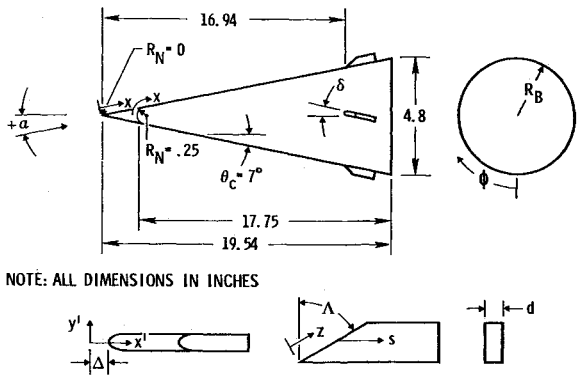

Fig. 1 Sketch of wind-tunnel model and coordinate system.

Experimental Techniques

The pressure sensing instrumentation used for this test was a 48-channel system containing Consolidated Control Corp. "Ultradyne" pressure transducers. The pressures were monitored during a run, with the data being taken when steady readings were obtained.

For the oil flow tests, a mixture of Dow Corning 200 and Zyglo Penetrant, Type ZL-22A, was used. A light coat of Dow Corning 200 was applied to the model, which was then sprayed with Zyglo. The initial temperature of the model was maintained between 90 and 100°F to ensure that the oil flowed well. Illumination of the model with an ultraviolet light source caused the Zyglo to fluoresce, which provided excellent contrast between the model and the oil. Photographic coverage was obtained with a Polaroid camera mounted on top of the tunnel.

Two types of heat-transfer measurements were made. Leading-edge heat transfer was obtained with the transient thin-skin technique using Chromel-Alumel thermocouples (skin thickness =0.030″). Data were taken at a sampling rate of 57 times/sec when the model reached the nozzle flowfield core. A curve fit through fifteen consecutive points then yielded the heat-transfer rate from the relation

$$\dot{q} = \rho\, c\, b\, dT/dt$$

The values thus obtained were corrected for conduction errors.[21] Heat-transfer coefficients were obtained assuming a laminar recovery factor of 0.85.

Heat-transfer measurements on the fin side and on the cone in the vicinity of the fin were obtained with the phase change paint technique.[22] Details concerning phase change paint testing in the AFFDL facility are contained in Ref. 23.

III. Flowfield Visualization

Results from the flowfield visualization phase of the program are presented in this section. First, a general discussion of flow over inclined cones is given. Then the characteristics of the fin induced interaction are considered. In both cases the results are compared with earlier experimental work. The section is concluded with a discussion of the observed shock wave patterns.

Angle-of-Attack Induced Separation

Hypersonic flow over an inclined cone has been the subject of a number of experimental investigations[1–7] in recent years, and the general features of such a flow are fairly well understood. At no angle of attack, the flowfield and pressure distribution are axisymmetric. As the cone angle of attack is increased, a minimum in the circumferential pressure occurs. The adverse pressure gradient following the minimum causes the boundary layer to separate from the leeward side of the cone, forming a pair of symmetrical, helical vortices. The separation may or may not be accompanied by the appearance of imbedded shock waves. Stetson and Odjana[6] have identified two types of cone leeward side separation. In the first type, there is no communication between the base and leeward side regions of the cone. This type of separation is analogous to that which would be expected for an infinitely long cone. In the second type, known as the base interference case, there is communication between the two regions, and the flow is characterized by equal leeward side and base pressures.

In the present tests the boundary layer separated along a conical ray, and as the angle of attack increased the separation line moved further from the leeward meridian. Surface streamlines in the separated region diverge from the leeward meridian and converge to the separation line. Photographs of the observed separation patterns are presented in Ref. 24.

Leeward side separation locations from the present study and several earlier references[4–6] are correlated in Fig. 2.

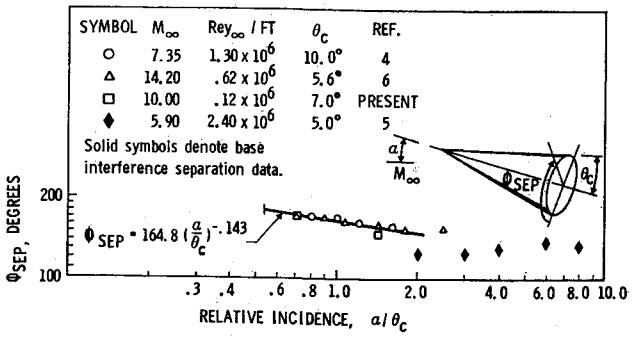

Fig. 2 Correlation of sharp cone leeward side separation location.

The separation location ϕ_{sep}, measured from the windward meridian, is correlated in terms of the relative incidence $\alpha/\theta c$ of the cone. For $\alpha/\theta c < 2$, the data are correlated to within $\pm 5\%$ by the expression $\phi_{sep} = 164.8\ (\alpha/\theta c)^{-0.143}$, and appear to be independent of freestream Reynolds number. For $\alpha/\theta c \geq 2$, the measurements of Stetson and Odjana show the separation location constant, whereas the data of Feldhuhn et al., show a movement of the separation line toward the leeward meridian with increased $\alpha/\theta c$. Whether this behavior is a Mach and Reynolds number effect or a characteristic of base interference separation is not clear.

Fin Induced Separation

Consider now the fin induced separation patterns on the cone. Figures 3 and 4 are typical photographs obtained during the present tests.

It is apparent from Figs. 3 and 4 that the separation patterns are quite dependent on freestream Reynolds number. The forward extent of separation is small, and it increases with increasing Reynolds number, as has been observed for an unswept fin mounted on a flat plate.[8] The lateral separation is extensive and also increases with increasing Reynolds number.

For no fin cant, the basic Reynolds number effect is on the scale of the separation. The surface streamline patterns for both Reynolds numbers show a broad region aft of the initial separation line in which the stream-line directions are nearly parallel to the separation line. Between this area and the fin-cone corner, a region of high shear exists. Based upon earlier corner flow studies, it is believed the high shear is the result of a vortex located in the corner region.

For a fin cant of 10°, Reynolds number affects both the scale of the separation and the surface streamline patterns aft of separation. For $Rey_{\infty,L} = 0.2 \times 10^6$, the patterns are similar to those observed for no fin cant; for $Rey_{\infty,L} = 1 \times 10^6$, the flow aft of the separation line is altered considerably from the low Reynolds number case. On the windward side of the fin, there is a region of strong outflow immediately behind the separation line. This region is followed by two high shear regions between which a secondary separation region exists. The first high shear area is nearly uniform with chordwise distance; the second, however, is most intense in the fin wake region. The fin leeward side is characterized by a single high shear region which extends from the leading edge of the fin to the cone base region.

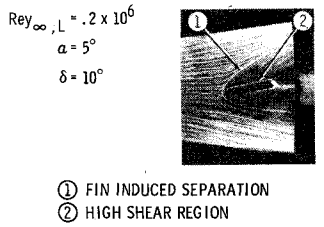

Fig. 3 Low Reynolds Number oil flow pattern.

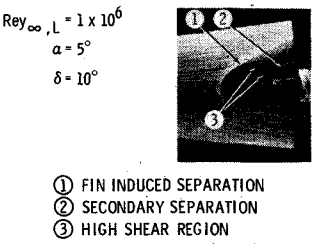

Fig. 4 High Reynolds Number oil flow pattern.

In their recent corner flow study West and Korkegi[17] also observed that the flowfield structure varied significantly with Reynolds number (for $Rey < 3 \times 10^6$), which they attributed to the dominant influence of viscid-inviscid interaction and boundary-layer displacement effects.

The initial separation line is of interest because, as will be seen shortly, if this contour can be predicted, estimates of the pressure in the separated region can be made. In Fig. 5, the lateral extent of separation y'/d is plotted against the axial distance x'/d, where d is the fin diameter. The data are described quite well by the equation $y'/d = c\ Rey_{c,x}^{1/4}\ (x'/d)^{1/2}$ where $c = 0.045$. In general, one would expect the constant c to be a function of fin sweep.

The present results for separation contours can be compared with those obtained by Ball[25] for finite span flaps. In Ref. 25, it was observed that the separation contours had a spatial dependence of the form $y' = \bar{\chi}^{-1/2}\ F(\bar{\chi}, M, \delta)x'^{1/3}$, where $\bar{\chi} = M^3/(Rey_x)^{1/2}$ is the viscous interaction parameter, and F is an empirically determined function of $\bar{\chi}$, Mach number M, and flap deflection δ. The function $F(\bar{\chi}, M, \delta)$ occurred as a result of choosing the forward extent of separation as the characteristic dimension for nondimensionalizing x'. In the present tests, this distance was clearly a function of shock layer Mach and Reynolds numbers. However, its accurate experimental determination was not possible. For this reason, the fin diameter was selected as the characteristic length. This choice resulted in the equation $y'/d = c\ Rey_x^{1/4}/(x'/d)^{1/2}$. Had the separation length been utilized, the initial separation line contour could have been expressed as $y' = \bar{\chi}^{-1/2}\ G(\bar{\chi}, M, \Lambda)x'^{1/2}$. Thus, although fin induced and flap induced separation patterns exhibit the same basic Reynolds number scaling through the parameter $\bar{\chi}$, their spatial dependences differ.

Schlieren Observations

Schlieren photographs were taken during the high Reynolds number runs for $r_n = 0$ and 0.25, and $\alpha = 0°$, 5°, and 10°. For all cases, the fin shock was nearly parallel to the fin leading edge, which suggests that infinite swept cylinder theories may be utilized to predict leading-edge pressures and

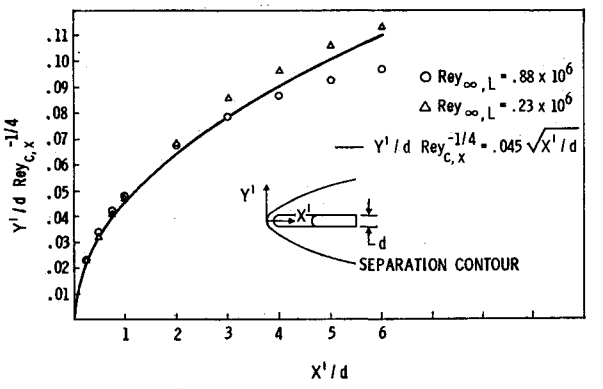

Fig. 5 Fin induced separation contours.

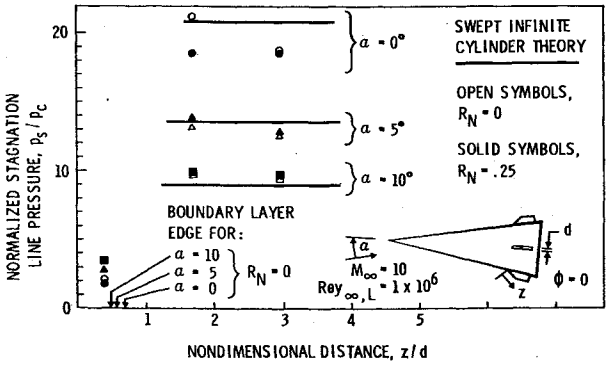

Fig. 6 Fin stagnation line pressures.

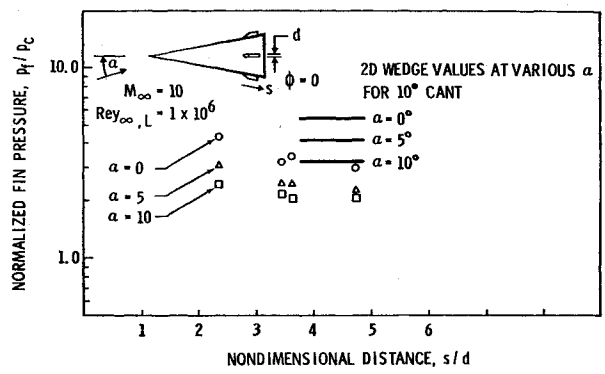

Fig. 8 Fin side pressure for $\delta = 10°$.

heat-transfer coefficients. There was not evidence of any shock interference which would lead to increased heat transfer to the leading edge. Theoretical calculations[26] substantiated this observation.

IV. Pressure Measurements

Results from the pressure phase of this study are presented in this section. Leading-edge pressures are compared with swept infinite cylinder theory and fin side pressures are compared with the theoretical predictions of Creager.[27] The section is concluded with a discussion of the pressures in the fin-cone corner region.

Fin Leading Edge Pressure

Stagnation line pressure data are presented in Fig. 6. Theoretical infinite cylinder values for the pressure are based upon flow conditions just upstream of the fin obtained with the equivalent cone approximation. Outside of the boundary layer, agreement with theory is good; within the region influenced by the cone boundary layer lower pressures are measured. Additional data obtained at a reduced freestream Reynolds number indicated reduced pressure in the region influenced by the cone boundary-layer thickness.

It has been observed by Coleman and Lemmon[28] that end effects can cause the leading-edge pressures on small fins to be higher than the swept infinite cylinder value. This phenomenon is a function of z/d and the Mach number of the approaching flow. For the present data, end effects appear to be confined to the boundary-layer region, which would be expected because of the relatively high cone Mach numbers ($6 \sim 8$) and small fin diameter. Attempts to calculate the pressures influenced by the boundary layer utilizing the method proposed in Ref. 28 were not successful, probably due to the unknown boundary-layer profiles resulting from separation ahead of the fin.

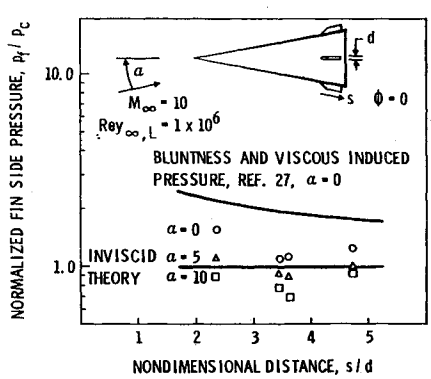

Fig. 7 Fin side pressures for $\delta = 0°$

Fin Side Pressures

Figure 7 presents measurements obtained in the windward ($\phi = 0°$) meridional plane for no fin cant. Also shown on this figure is the bluntness and viscous induced pressure distribution predicted by the theory of Creager.[27] The data suggest that viscous and bluntness effects are present, but that they are modified by end losses due to the short span of the fin. Angle of attack lessens these effects because of the increased Reynolds number and decreased Mach number in the shock layer.

Data for a fin cant of 10° are presented in Fig. 8. The results again suggest that viscous and bluntness effects are important. Shown for comparison purposes are the inviscid pressures which would be obtained by a two-dimensional deflection of 10°. The pressures for the fin configuration are approximately one-half of these values. Data were not obtained on the fin leeward side, but it is anticipated that leeward pressures would be dominated by viscid-inviscid effects.

Fin side pressures were also obtained in the $\phi = 90°$ meridional plane. The crossflow induced by angle of attack resulted in an effective fin cant greater than the geometric cant. For $\delta = 0°$ and $\alpha = 10°$, the fin side pressures were comparable to those observed for $\delta = 10°$ and $\alpha = 0°$.

Fin-Cone Corner Region Pressures

Typical results obtained on the cone in the vicinity of the fin are tabulated in Fig. 9. The fin induced separation results in increased pressure in the corner region. The pressure increase is essentially the same for both $\delta = 0$ and 10°, which suggests the pressure rise is the result of a free-interaction.

It was observed by West and Korkegi in their recent corner flow study that three-dimensional boundary-layer separation

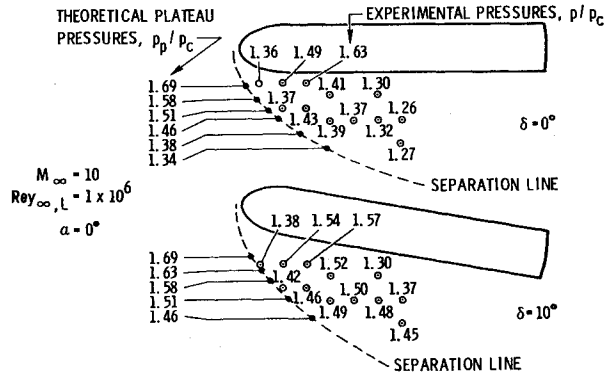

Fig. 9 Cone pressures in vicinity of fin.

may be thought of as a two-dimensional interaction with a strong crossflow. By utilizing this analogy and the plateau pressure correlation of Ref. 29, very good agreement may be obtained with their experimental data when the Mach and Reynolds numbers required for correlation are based upon flow conditions normal to the separation line. Applying this method to the present configuration yielded the values indicated ahead of the separation contours. In general, the agreement is good. It should be noted that this technique tended to overpredict the pressures observed at $Rey_{\infty,L} = 0.2 \times 10^6$. The reason for this is not clear; it could be that the plateau pressure location was shifted aft of the instrumentation, or that the agreement for $Rey_{\infty,L} = 1.0 \times 10^6$ was fortuitous.

V. Heat-Transfer Measurements

Data from the heat-transfer phase of the program are discussed in this section. Leading-edge heat-transfer coefficients are compared with swept infinite cylinder theoretical predictions. Fin side heating data are presented and compared with blunt swept slab predictions. Heat-transfer coefficients from the fin-cone corner region are presented and compared with experimental results from corner flow studies.

Fin Leading Edge Heat Transfer

Leading-edge heat-transfer coefficients are presented in Fig. 10. Also shown on this figure are the geometric intersection points of the cone boundary layer with the fin leading edge. Out of the region of boundary-layer influence, the heat-transfer coefficients are predicted quite well by swept infinite cylinder theory.[30] Local properties in the shock layer required for this theory were obtained with the equivalent cone approximation. Note that an angle of attack of 10° results in only a 60% increase in leading-edge heating for the present configuration and test conditions. Data not shown indicate the effect of bluntness was to lower slightly the heat-transfer coefficient in the region influenced by the boundary layer.

Fin Side Heating

Fin side isoheating contours were obtained at the high Reynolds number condition for the sharp cone configuration at angles of attack of 0, 5 and 10°. The fin was mounted on the windward meridian. For $\alpha = 0°$ and 5°, the fin side heating was reasonably uniform, being slightly higher near the top of the fin. A cool region occurred near the bottom of the fin as a result of the cone boundary layer. At $\alpha = 10°$, a region of increased heating occurred near the cone on the aft portion of the fin. There was a general trend of increased side heating with increased angle of attack.

Data taken from the midspan of the fin for $\alpha = 0$ are compared with blunt, swept slab theory[31] in Fig. 11. Considering

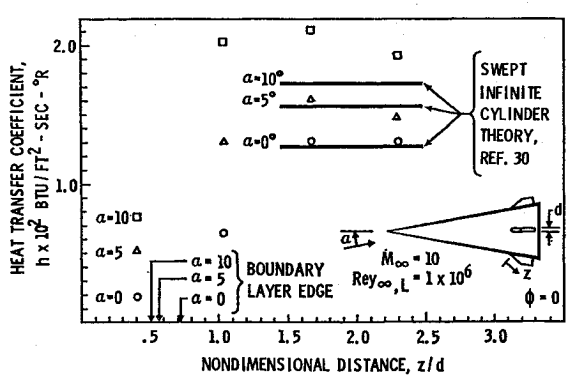

Fig. 10 Leading edge heat-transfer coefficients.

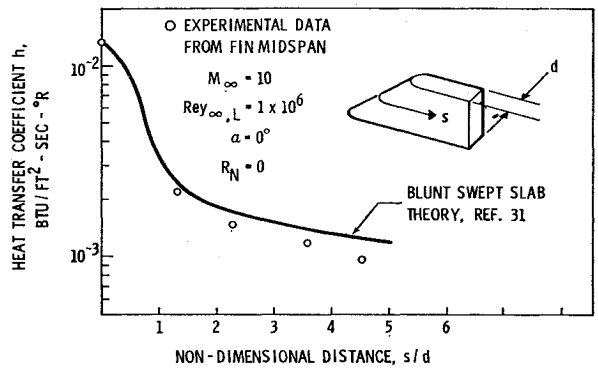

Fig. 11. Fin side heating compared with theory.

the short span of the present fin, the agreement with theory is quite good. As expected, the agreement becomes poorer near the trailing edge of the fin.

The effect of canting the fin 10° is illustrated in Fig. 12. A region of extremely high heating extends the length of the fin at a height just above the undisturbed cone boundary layer. Ablation patterns on the Teflon fin after long runs (~20 sec) suggest that this region of high heating originates near the stagnation line. It is doubtful that the peak heating rates were measured; the highest value measured was an order of magnitude higher than the $\delta = 0°$ value, and about a factor of five higher than the theoretical, undisturbed value for a 10° fin cant. Data were not obtained for $\alpha = 5°$ and 10°, but it is anticipated that the peak heating rates would increase with increasing angle of attack.

As noted by Stainback and Weinstein[13] the fact that the peak heating in a corner geometry is independent of a length scale indicates that an inviscid phenomenon (a vortex, or separation and reattachment, or a combination of the two) controls the peak heating.

Data were also taken in the $\phi = 90°$ meridional plane for $\alpha = 5°$ and 10°, and $\delta = 0°$. The effective cant of the fin due to crossflow resulted in heating patterns similar to those observed for a fin cant of 10°. Fin side isoheating contours for the cases mentioned above, but not presented herein, are presented in Ref. 24.

Fin-Cone Corner Region Heat Transfer

Data for no fin cant are presented in Fig. 13. A single region of high heat transfer originates near the leading edge of the fin and extends downstream nearly parallel to the fin. For $\alpha = 0$, the peak heating is a factor of seven higher than the undisturbed cone heating on the windward meridian. This value is comparable to the increase observed by Bertram and Henderson[32] for a 76° swept fin mounted on a sharp flat plate and aligned with the free-stream.

The effects of fin cant and angle of attack are illustrated in Fig. 14. At no angle of attack, a region of high heat transfer on the windward side of the fin originates near the trailing edge

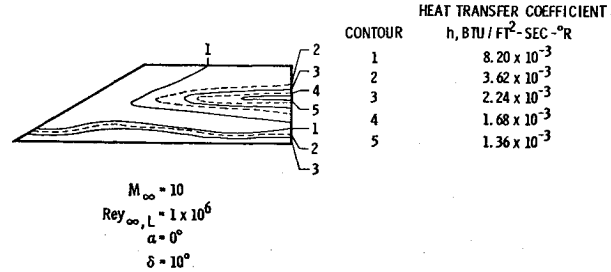

Fig. 12. Effect of cant on fin side heating.

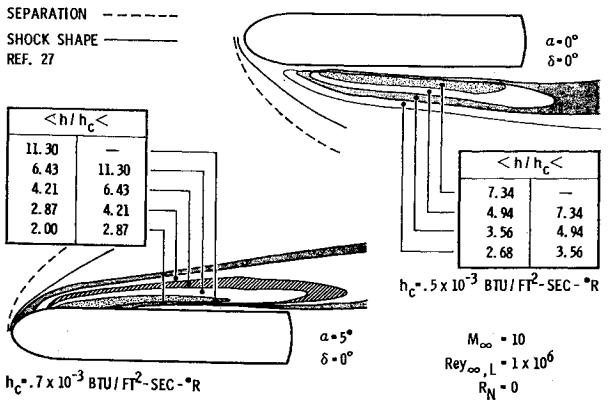

Fig. 13 Cone interference heating for $\delta = 0°$.

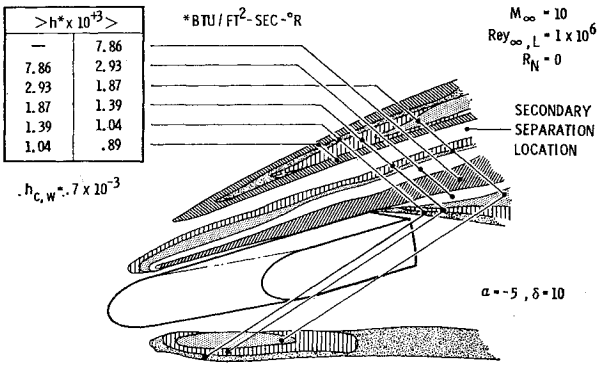

Fig. 15 Cross flow effects on cone interference heating.

of the fin and extends into the fin wake region. The heat transfer in this region is nearly an order of magnitude higher than the theoretical undisturbed cone value. Near the leading edge of the fin a second region exists in which the heat-transfer coefficients are a factor of five higher than the undisturbed value. Significant increases over local heat-transfer coefficients also exist on the leeward side of the fin.

Angle of attack results in a marked change in the interference heating contours. The most obvious change is the appearance of a second peak in the heat-transfer coefficient distribution in a direction normal to the fin. The minimum in heat transfer between the two peaks corresponds to the location of the secondary separation line discussed in conjunction with the oil flow results (Fig. 4). Aft of the leading edge, the distributions are essentially constant along conical rays. The two peaks in heating and the conical invariance are similar to the patterns observed in earlier corner flow studies. It is probable that the actual peaks in heat transfer were not measured; the highest heat-transfer rates measured were a factor of ten higher than the $\alpha = 0$ undisturbed heat transfer. Again significant increases over the undisturbed heat transfer were observed on the leeward side of the fin. At $\alpha = 10°$, two peaks in the leeward heating were present.

Interference heating patterns on the cone at the $\phi = 90°$ position are presented in Fig. 15. For this case, the fin is canted 10° and the cone angle of attack is $-5°$. This orientation leads to the greatest increase in heating over the undisturbed value due to the high effective fin cant which results from cross flow.

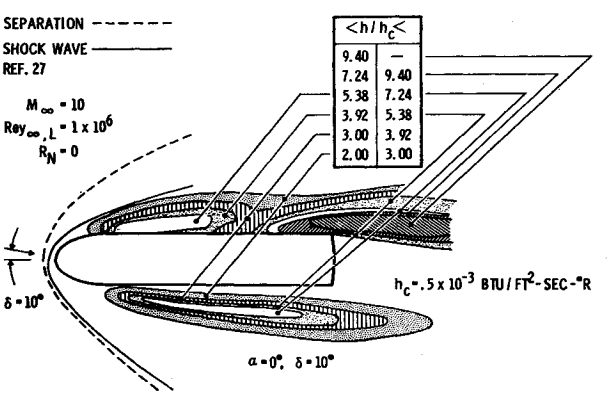

a)

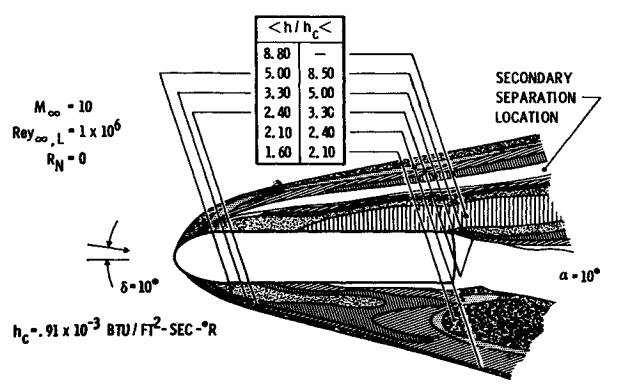

b)

Fig. 14 Cone interference heating for $\delta = 10°$.

Effect of Fin Geometry

Several different fin geometries were considered during this investigation. Of the factors considered, fin sweep had the most pronounced effect. For a fin sweep of 45° and cant of 10° the heating patterns in the fin region differed significantly from those for $\Lambda = 60°$. A region of high heating on the fin side originated near the leading edge and extended the length of the fin. However, for $\Lambda = 45°$ the vertical location of the peak varied with distance from the leading edge. Near the trailing edge a second, and higher, peak in heating occurred. The paint melt patterns suggested that a region of separated flow existed between the two peaks. The measured peaks were a factor of two lower than those observed on the $\Lambda = 60°$ fin. Isoheating patterns on the cone also differed from those characteristic of $\Lambda = 60°$. A single, fairly uniform region of high heating occurred at the fin-cone intersection. Again the magnitude of the peak was lower than for the $\Lambda = 60°$ configuration.

Isoheating patterns from a fin having a flat face were similar to those obtained on fins having a cylindrical leading edge, as were those taken on a fin having a diameter of 0.5 in.

VI. Conclusions

Angle of attack induced separation from the leeward side of the cone occurred along a conical ray. The extent of this separation may be predicted to within $\pm 5\%$ by the empirical expression $\phi_{sep} = 164.8\,(\alpha/\theta_c)^{-0.143}$ for $\alpha/\theta_c < 2$. The extent of separation appears to be independent of Reynolds number in the range $0.2 \times 10^6 < Rey\infty/\text{ft} < 1.2 \times 10^6$. For angles of attack greater than about twice the cone half-angle, the separation location is approximately constant.

The fin induced widespread separation on the cone. The forward extent of separation is small and depends upon th

local conditions ahead of the fin. The lateral extent of separation is correlated to within $\pm 5\%$ by the empirical expression

$$y'/d = 0.045\ Rey_x^{1/4}(x'/d)^{1/2}$$

The structure of the surface oil flow patterns is quite dependent upon Reynolds number, which earlier investigators have attributed to the dominant influence of viscid-inviscid and boundary-layer displacement effects. The patterns bear many similarities to those observed in corner flow studies. Schlieren photographs show no evidence of shock interference which would lead to increased fin leading-edge heating; theoretical calculations substantiate this observance.

Fin leading-edge pressures are predicted adequately with swept infinite cylinder theory based on shock layer properties obtained with the equivalent cone approximation. Lower pressures are observed near the cone surface due to viscous dissipation in the cone boundary layer.

Fin side pressures for $\delta = 0°$ show evidence of viscous and bluntness induced effects. Comparisons with the theoretical predictions of Creager suggest that these effects are reduced by the short span of the fin. Induced effects are also present for a fin cant of 10°; aft of the leading edge, fin side pressures are approximately one-half the value predicted by assuming a two-dimensional, 10° deflection.

Fin induced separation results in increased pressure on the cone surface. This increase can be predicted by a plateau pressure correlation, if flow properties are based upon conditions normal to the separation line.

Fin leading-edge heat-transfer coefficients agree with theoretical swept infinite cylinder predictions, if flow properties required for this theory are based upon shock layer conditions. For the present test conditions, 10° angle of attack resulted in a 60% increase in leading-edge heating.

For no fin cant and angles of attack of 0° and 5°, the fin side heating is reasonably uniform; at $\alpha = 10°$, an increase in heating at the fin-cone corner occurs. Fin midspan heat-transfer distributions for $\alpha = 0$ agree with blunt, swept slab predictions except near the fin trailing edge, where the experimental values are up to 30% lower than the theoretical predictions.

Canting the fin 10° results in a region of increased heat transfer which originates near the leading edge and extends the length of the fin. It is doubtful that the actual peak heat-transfer coefficients were observed; the values measured were an order of magnitude higher than those for no fin cant.

Isoheating contours on the cone are similar to those observed in corner flow studies. The combined effects of angle of attack and corner interference result in increases in heat transfer of up to a factor of twenty above the cone heating at no angle of attack.

Flattening the fin leading edge does not alter significantly the heat-transfer distributions in the fin-cone corner region. These distributions are dependent, however, upon the leading-edge sweep. For $\Lambda = 45°$, the fin side and cone surface distributions exhibit different spatial characteristics and are a factor of two lower in magnitude than the $\Lambda = 60°$ results.

References

[1] Fitch, C. R., Morris, S. D., and Dunkin, O. L., "Force, Pressure, and Heat Transfer Tests on the G. E. Skybolt Nose Cone at Mach 10," AEDC-TDR-62-125, 1962, Arnold Engineering Development Corp., Arnold Air Force Station, Tenn.

[2] Anderson, J. D., Jr., "Hypersonic Viscous Flow Over Cones at Nominal Mach 11 in Air," ARL 62-387, 1962, Aerospace Research Labs., Wright-Patterson Air Force Base, Ohio.

[3] Tracy, R. R., "Hydpersonic Flow Over a Yawed Circular Cone," GALCIT Hypersonic Research Project Memo 69, 1963, Graduate Aeronautical Lab., California Institute of Technology, Pasadena, Calif.

[4] George, O. L., "An Experimental Investigation of the Flow Field Around an Inclined Sharp Cone in Hypersonic Flow," SC-RR-69-577, Sept. 1969, Sandia Lab., Albuquerque, N. Mex.

[5] Feldhuhn, R. H., Winkelmann, A. E., and Pasiuk, L., "An Experimental Investigation of the Flowfield Around a Yawed Cone," *AIAA Journal*, Vol. 9, No. 6, June 1971, pp. 1074–1081.

[6] Stetson, K. F. and Ojdana, E. S., "Boundary-Layer Separation on Slender Cones at Angle of Attack," *AIAA Journal*, Vol. 10, No. 5, May 1972, pp. 642–648.

[7] Hortstmann, C. C. and Kussay, M. I., "Hypersonic Viscous Interaction on Slender Cones," *AIAA Journal*, Vol. 6, No. 12, Dec. 1968, pp. 2364–2371.

[8] Young, F. L., Kaufman, L. G., II, and Korkegi, R. H., "Experimental Investigation of Interactions between Blunt Fin Shock Waves and Adjacent Boundary Layers at Mach Numbers 3 and 5," ARL 69-0214, Dec. 1968, Aerospace Research Labs., Wright-Patterson Air Force Base, Ohio.

[9] Thomas, J. P., "Flow Investigation About a Fin Plate Model at a Mach Number of 11.26," ARL 67-0188, Sept. 1967, Aerospace Research Labs., Wright-Patterson Air Force Base, Ohio.

[10] Bushnell, D. M., "Interference Heating on a Swept Cylinder in the Region of Its Intersection with a Wedge in Hypersonic Flow," TN D-3094, 1965, NASA.

[11] Hiers, R. S. and Loubsky, W. J., "Effects of Shock-Wave Impingement on the Heat Transfer on a Cylindrical Leading Edge," TN D-3859, Feb. 1967, NASA.

[12] Charwat, A. F. and Redekopp, L. G., "Supersonic Interference Flow Along the Corner of Intersecting Wedges," *AIAA Journal* Vol. 5, No. 3, March 1967, pp. 480–488.

[13] Stainback, P. C. and Weinstein, L. M., "Aerodynamic Heating in the Vicinity of Corners at Hypersonic Speeds," TN D-4130, Nov. 1967, NASA.

[14] Watson, R. D. and Weinstein, L. M., "A Study of Hypersonic Corner Flow Interactions," *AIAA Journal*, Vol. 9, No. 7, July 1971, pp. 1280–1286.

[15] Gulbran, C. E., Redeker, E., Miller, D. S., and Strack, S. L., "Heating in Regions of Interfering Flow Fields," AFFDL-TR-65-49, March 1967, Air Force Flight Dynamics Lab., Wright-Patterson Air Force Base, Ohio.

[16] Neumann, R. D. and Burke, G. L., "The Influence of Shock Wave Boundary Layer Effects on the Design of Hypersonic Aircraft," AFFDL TR-68-152, March 1969, Air Force Flight Dynamics Lab., Wright-Patterson Air Force Base, Ohio.

[17] West, J. E. and Korkegi, R. H., "Supersonic Interaction in the Corner of Intersecting Wedges at High Reynolds Numbers," *AIAA Journal*, Vol. 10, No. 5, May 1972, pp. 652–656.

[18] Korkegi, R. H., "Survey of Viscous Interactions Associated with High Mach Number Flight," *AIAA Journal*, Vol. 9, No.5, May 1971, pp. 771.

[19] Czysz, P., "The High Temperature Hypersonic Gasdynamics Facility Estimated Mach Number 6 Through 14 Performance," ASD-TDR-63-456, June 1963, Air Force Flight Dynamics Lab., Wright-Patterson Air Force Base, Ohio.

[20] Smith, R. R. and Dahlem, V., "Performance Estimates for the AFFDL Pebble Bed Heated Hypersonic Wind Tunnel," FDM-TM 57-3, July 1967, Air Force Flight Dynamics Lab., Wright-Patterson Air Force Base, Ohio.

[21] Meleason, E. T. and Burke, G. L., "Experimental Determination of Conduction Errors in Aerodynamic Heating Test Data," ASRMDF TM-62-37, June 1962, Air Force Flight Dynamics Lab., Wright-Patterson Air Force Base, Ohio.

[22] Jones, R. A. and Hunt, J. L., "Use of Fusible Temperature Indicators for Obtaining Quantitative Aerodynamic Heat Transfer Data," TR-R-230, Feb. 1966, NASA.

[23] Patterson, J. L., "Heat Transfer Testing in the AFFDL High Temperature Facility Using the Phase Change Coating Technique," FXG-TM-70-12, Aug. 1970, Air Force Flight Dynamics Lab., Wright-Patterson Air Force Base, Ohio.

[24] Bramlette, T. T., "Flow Field, Pressure, and Heat Transfer Associated with Small Fins in Laminar Hypersonic Flow," SCL-RR-720339, Nov. 1972, Sandia Lab., Livermore, Calif.

[25] Ball, K. O. W., "A Summary of Factors Influencing the Extent of Separation of a Laminar Bounday Layer due to a Compression Corner at Moderately Hypersonic Speeds," ARL 71-0065, April 1971, Aerospace Research Lab., Wright-Patterson Air Force Base, Ohio.

[26] Edney, B. E., Bramlette, T. T., Ives, J., Hains, F. D., and Keyes, J. W., "Theoretical and Experimental Studies of Shock Interference Heating," Rept. 9500-920-195, Oct. 1970, Bell Aerospace Co., Buffalo, N.Y.

[27] Creager, M. O., "The Effect of Leading-Edge Sweep and Surface Inclination on the Hypersonic Flow Field Over a Blunt Flat Plate," Memo 12-26-58A, Jan. 1959, NASA.

[28] Coleman, H. W. and Lemmon, E. C., "Turbulent Heat Transfer and Pressure on Leading Edges of Fins Mounted on a Cone," SCL-RR-720308, 1972, Sandia Lab., Livermore, Calif.

[29] Markarian, C. F., "Heat Transfer in Shock Wave Boundary Layer Interaction Regions," NWC TP 4485, Nov. 1968, Naval Weapons Center, China Lake, Calif.

[30] Beckwith, I. E. and Gallagher, J. J., "Local Heat Transfer and Recovery Temperatures on a Yawed Cylinder at Mach Number of 4.15 and High Reynolds Numbers," TR R-104, 1958, NASA.

[31] Hunt, J. L., Bushnell, D. N., and Beckwith, I. E., "The Compressible Turbulent Boundary Layer on a Blunt Swept Slab With and Without Leading-Edge Blowing," TN D-6203, March 1971, NASA.

[32] Bertram, M. H. and Henderson, A., Jr., "Some Recent Research With Viscous Interacting Flow in Hypersonic Streams," *Proceedings of the Symposium on Viscous Interaction Phenomena in Supersonic and Hypersonic Flow*, Hypersonic Research Labs., Aerospace Research Labs., May 1969, pp. 1–30.

NOVEMBER 1973 J. SPACECRAFT VOL. 10, NO. 11

Static Stability and Drag Studies for Bodies of Revolution in Supersonic Flow

HANS-JOACHIM LUCKERT*
Space Research Corporation, Montreal, Quebec, Canada

Reliable estimates of stability and performance characteristics are essential for the design of missiles, shells, and space probes. Particularly in the case of parametric studies to determine the optimum configuration for a specific mission, an inexpensive and simple method is needed. The second-order shock expansion theory of Syvertson and Dennis was found to meet these requirements. The method, somewhat modified for concave corners, was therefore used in practical applications for bodies of revolution in axisymmetric flow. Example calculations show the usefulness of the method for comparison of configurations, such as ogival and parabolic, or tangent and secant contours. Applied to configurations with flares considerable differences from conventional results with the Newtonian theory were obtained; the differences depend strongly on Mach number, flare length and angle. A further application deals with the effect of forebody on afterbody. Comparison with test results confirm the predictions. The method is therefore especially useful for preliminary design studies for which more sophisticated theories or experimental programs would be uneconomical regarding cost and time.

Nomenclature

a, b = constants in equation for pressure [Eq. (2)]
C_1 = characteristic coordinate
C_{DW} = wave drag coefficient = Drag/$[(\gamma/2)M_\infty{}^2 p_\infty S_{\text{ref}}]$
C_N = normal force coefficient=Normal Force /$[(\gamma/2)M_\infty{}^2 p_\infty S_{\text{ref}}]$
$C_{N\alpha}$ = $\partial C_N/\partial\alpha$
d, D = diameter
f = fineness ratio ($=L/D$)
K_D = ballistic drag force coefficient = $(\pi/8)C_D$
K_N = ballistic normal force coefficient = $(\pi/8)C_{N\alpha}$
l, L = length
M = Mach number
p = pressure
r, R = radius
s = coordinate along body contour
S = cross section area
s_g = gyroscopic stability factor
x, x' = coordinate along body axis from nose (x) or tail (x')
α = angle of attack, rad
γ = ratio of specific heats ($=1.4$)
δ = semivertex angle, deg
μ = Mach angle
ξ = contour coordinate, $= x/L$
η = contour coordinate, $= d/D = r/R$

Subscripts

1, 2, 3, 4 = positions on body
c = cone
tc = tangential cone of body element
cp = center of pressure
ref = reference
B = base
S = secant
T = tangent

Presented as Paper 73-295 at the AIAA 3rd Sounding Rocket Technology Conference, Albuquerque, N. Mex., March 7–9, 1973; submitted March 29, 1973; revision received June 27, 1973.

Index categories: LV/M Aerodynamics; Aircraft Configuration Design.

* Chief Aerodynamicist. Associate Fellow AIAA.

Introduction

MISSILES, upper atmosphere research vehicles, and shells have the principal requirements of reaching a given altitude or range with a certain degree of aerodynamic or gyroscopic stability. In either case it is essential to predict the stability chracteristics, the normal force curve slope and the center of pressure, as well as the drag as accurately as possible in order to achieve the most suitable configuration for the given requirements.

The present study deals only with bodies of revolution in symmetric flow. Various design charts and handbooks are available to estimate the required aerodynamic characteristics for simple configurations, such as cone-cylinder or ogive-cylinder combinations, conical flares, or boattails.[1-3] Some